

Valley Splitting in Silicon from the Interference Pattern of Quantum Oscillations

M. Lodari¹, L. Lampert,² O. Zietz,² R. Pillarisetty,² J. S. Clarke,² and G. Scappucci^{1,*}

¹*QuTech and Kavli Institute of Nanoscience, Delft University of Technology,
Post Office Box 5046, 2600 GA Delft, Netherlands*

²*Intel Components Research, Intel Corporation, 2501 NW 229th Avenue, Hillsboro, Oregon 97124, USA*



(Received 9 December 2021; accepted 5 April 2022; published 29 April 2022)

We determine the energy splitting of the conduction-band valleys in two-dimensional electrons confined in silicon metal oxide semiconductor Hall-bar transistors. These silicon metal oxide semiconductor Hall bars are made by advanced semiconductor manufacturing on 300 mm silicon wafers and support a two-dimensional electron gas of high quality with a maximum mobility of $17.6 \times 10^3 \text{ cm}^2/\text{Vs}$ and minimum percolation density of $3.45 \times 10^{10} \text{ cm}^{-2}$. Because of the low disorder, we observe beatings in the Shubnikov–de Haas oscillations that arise from the energy splitting of the two low-lying conduction band valleys. From the analysis of the oscillations beating patterns up to $T = 1.7 \text{ K}$, we estimate a maximum valley splitting of $\Delta E_{\text{VS}} = 8.2 \text{ meV}$ at a density of $6.8 \times 10^{12} \text{ cm}^{-2}$. Furthermore, the valley splitting increases with density at a rate consistent with theoretical predictions for a near-ideal semiconductor-oxide interface.

DOI: [10.1103/PhysRevLett.128.176603](https://doi.org/10.1103/PhysRevLett.128.176603)

Electron spin qubits in silicon quantum dots are a compelling candidate for quantum processors because they have long coherence time [1–6], can operate quantum logic above one Kelvin [7,8], thereby providing scope for integration of classical control electronics [9], and leverage advanced semiconductor manufacturing [10]. To accelerate the device fabrication or measurement cycle towards larger quantum processors, it is crucial to characterize with high throughput the key electrical properties of the material, such as mobility, percolation density, and valley splitting energy. While mobility and percolation density are well-established metrics to qualify disorder in materials hosting spin qubits [11,12], measurements of valley splitting energy in silicon remains challenging. Quantum confinement across a (001) interface removes the sixfold degeneracy of the conduction-band valleys in Si [Fig. 1(a)] [13,14]. A twofold degenerate ground state is formed from the two out-of-plane valleys that present the heavy longitudinal effective mass of Si oriented along the quantization axis. The remaining twofold valley degeneracy is further lifted by the presence of a sharp confinement potential [15,16] and valley splitting quantifies the relevant energy separation.

Valley splitting is measured in quantum dot (QD) devices or in Hall bars field effect transistors. In a typical QD measurement, the single-particle energy level splitting is obtained by monitoring the increase in spin relaxation at the hot-spot [17,18]. These measurements are critical for developing functional qubits and give important insights on the small-scale variation of valley splitting at the device level. Alternatively, measurements in Hall bars probe the energy splitting of the two low-lying conduction-band

valleys in 2DEGs. Because of the different confinement experienced by electrons, Hall bar measurements are not a direct probe of valley splitting in qubits, but are still a useful quick turn monitor for high-throughput characterization and materials optimization. However, the evaluation of valley splitting in Hall bars relies on activation energy measurements in the quantum Hall effect (QHE) regime [16]. Because of the large magnetic field needed to overcome the Landau level broadening, enhancement of energy gaps is observed [19], making a direct comparison to the single-particle energy levels of QDs challenging. Furthermore, the complex electrostatics of quantum Hall edge states must be taken into account to correctly interpret the measurements [20].

In this Letter we determine valley splitting in silicon by analyzing the quantum interference properties of 2DEGs measured in magnetotransport. These measurements are performed in low-disorder silicon metal oxide semiconductor (Si-MOS) Hall bars. At a density greater than $3.7 \times 10^{12} \text{ cm}^{-2}$, the large vertical electric field increases valley splitting above the disorder-induced single-particle energy level broadening, thereby making visible the subtle interference effects due to quantum transport through the two energy-split valleys.

The Si-MOS Hall bars are fully optically patterned, feature a composite $\text{SiO}_2/\text{high-}\kappa$ thin dielectric and are made in a 300 mm wafer process line using the quantum dot process flow described in Refs. [10,21]. The width of the Hall bars is $6 \mu\text{m}$ and the interval between voltage terminals is $30 \mu\text{m}$. Magnetotransport characterization was performed at $T = 1.7 \text{ K}$ and at $T = 65 \text{ mK}$ in refrigerators equipped with cryomultiplexers [12] using standard

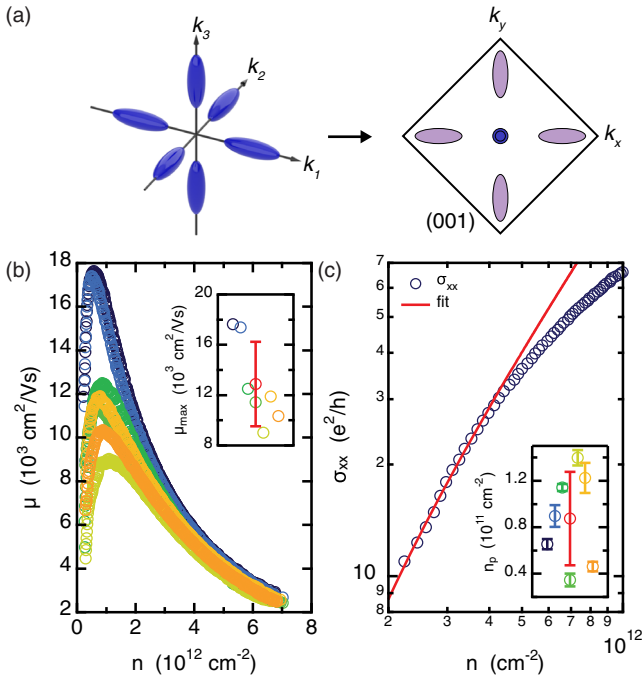


FIG. 1. (a) Schematic of the constant-energy ellipsoids for the Si conduction bands in momentum space (left cartoon) and constant energy ellipses obtained by two-dimensional (2D) projection for the (001) Si surface (right cartoon). Lower energy subbands are shown in blue. Long and short axis of the ellipsoids correspond to the longitudinal ($m_l = 0.92m_0$) and transverse ($m_t = 0.19m_0$) effective mass for electrons in Si, respectively. States from the out-of-plane valleys have the heaviest effective mass (m_l) along the quantization axis and form a double-degenerate ground state in two dimensions (concentric ellipses), further split in energy by the sharp confinement potential. (b) Mobility μ as a function of density n_H from Hall bar devices across a wafer at $T = 1.7 \text{ K}$. Circles colored in black, blue, green, light green, yellow, orange, and dark orange correspond to measurement from devices A–G, respectively. The inset shows the maximum mobility μ_{max} from all the devices and average value \pm standard deviation (red). (c) Conductivity σ_{xx} as a function of n_H from device (dark blue circles) with fit to percolation theory in the low density regime (red line). The inset shows the percolation density n_p from all the devices and average value \pm standard deviation (red).

four-probe low-frequency techniques with excitation source-drain bias of 1 mV. A positive bias applied to the gate (V_g) induces a 2DEG at the semiconductor-oxide interface.

Figure 1(b) shows the mobility-density curves at $T = 1.7 \text{ K}$ for seven devices A–G across the same wafer. The mobility increases as a function of density, due to the increased screening of scattering from impurities, until a peak is observed (μ_{max}). At higher density, surface roughness scattering at the semiconductor-oxide interface dominates and the mobility decreases [11]. The uniform mobility measured across devices at high density points to a

semiconductor-oxide interface with uniform properties across the wafer. Peak mobility and percolation density characterize disorder in the system at high and low density, respectively [11,22]. Device A (dark blue) and B (blue) show very high peak mobility ($\mu_{\text{max}} = 17.6$ and $17.4 \times 10^3 \text{ cm}^2/\text{Vs}$, respectively) at low density ($n_H = 5.75$ and $4.96 \times 10^{11} \text{ cm}^{-2}$, respectively). The inset in Fig. 1(b) shows a box plot of the peak mobility across the devices, with an average peak mobility $\mu_{\text{max}} = (12.9 \pm 3.4) \times 10^3 \text{ cm}^2/\text{Vs}$. The percolation density n_p is extracted from a percolation fit [23] of the density-dependent conductivity $\sigma_{xx} \sim (n_H - n_p)^p$ [Fig. 1(c)], device A, with $p = 1.31$ fixed for a 2D system [23,24]. The inset in Fig. 1(c) shows a box plot of the obtained n_p for all devices. We obtain a very low minimum n_p of $(3.5 \pm 0.4) \times 10^{10} \text{ cm}^{-2}$ with an average value of $(8.7 \pm 4.0) \times 10^{10} \text{ cm}^{-2}$. Overall, the maximum mobility in these Hall bars matches the highest values reported for Si-MOS devices with sub 10 nm oxide thickness from Ref. [25]. Most importantly, we set the benchmark for percolation density, which is the significant metric for disorder since quantum dot qubits operate in the low-density regime [25,26].

We now proceed to evaluate valley splitting from the quantum interference properties of magnetotransport. We focus on three devices (A, B, and C), with various degrees of disorder characterized by μ_{max} in the range of 12.5 to $17.6 \times 10^3 \text{ cm}^2/\text{Vs}$ and n_p in the range of 6.5 to $11 \times 10^{10} \text{ cm}^{-2}$. Figure 2(a) shows a typical magnetoresistivity curve from device B measured at 65 mK and at a density near peak mobility. The longitudinal resistivity ρ_{xx} shows Shubnikov–de Haas oscillations (SdH) and Zeeman splitting at magnetic field $B > 0.6$ and 3.5 T , respectively. At higher magnetic field the oscillation minimum goes to zero, confirming high-quality quantum transport [27]. Figure 2(b) shows the SdH oscillations amplitude $\Delta\rho_{xx}$ measured at $T = 1.7 \text{ K}$ as a function of $1/B$ and at increasing density. At lower densities (dark blue curve), the oscillations are periodic in $1/B$ and their amplitude increases following an exponential envelope, a clear indication of conduction through a single channel. As the 2DEG density increases (blue to orange curves), the oscillation frequency increases and a beating pattern is developed at a relatively low field ($\sim 2 \text{ T}$). The beating pattern features a full modulation of the oscillations amplitude at 1.7 K and reveals nodes with a position shifting toward higher magnetic fields B as V_g increases. This interference pattern is a signature of two parallel channels with similar high mobility contributing to transport. We attribute the origin of these channels to the two low-lying conducting band valleys in Si, since the valley splitting energy should dominate at low fields over cyclotron and Zeeman energy [28,29].

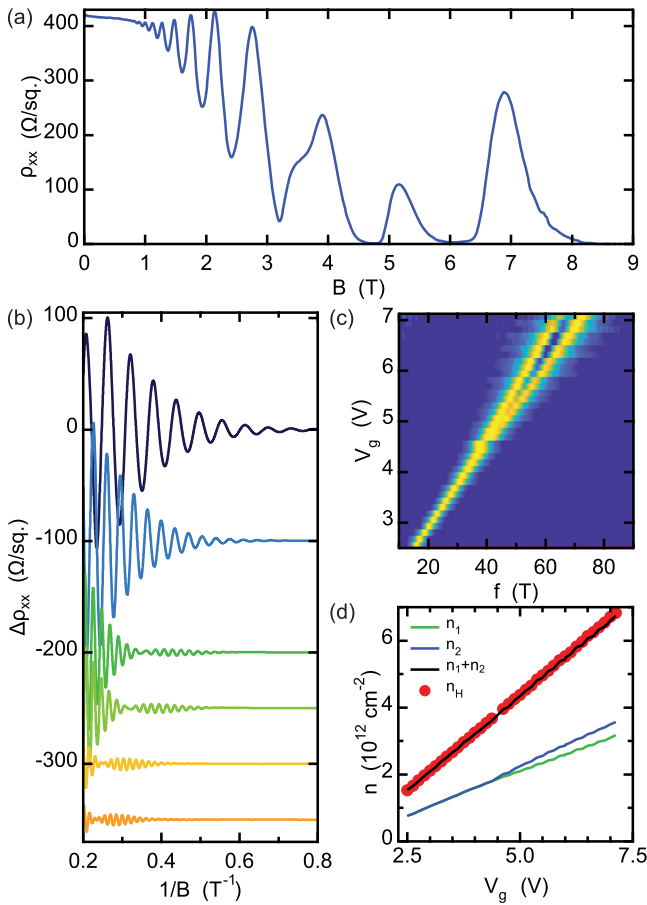


FIG. 2. (a) Longitudinal resistivity ρ_{xx} for device B as a function of magnetic field B at a Hall density $n_H = 9.3 \times 10^{11} \text{ cm}^{-2}$ and mobility $\mu = 16.1 \times 10^3 \text{ cm}^2/\text{Vs}$ at $T = 65 \text{ mK}$. (b) Oscillation amplitude $\Delta\rho_{xx} = \rho_{xx} - \rho_0$, where ρ_0 is the low field resistivity, as a function of the inverse perpendicular magnetic field $1/B$ for device B after smoothing and polynomial background subtraction at $T = 1.7 \text{ K}$. Different curves correspond to different and increasing accumulation gates V_g (dark blue to orange, respectively): $V_g = 2.6, 3.6, 5.1, 5.5, 6.5, \text{ and } 6.9 \text{ V}$ corresponding to $n_H = 1.7, 2.8, 4.5, 5.0, 6.1, \text{ and } 6.5 \times 10^{12} \text{ cm}^{-2}$. The curves are offset for clarity. (c) The normalized fast Fourier transform spectra amplitude of the oscillations for device (B) as a function of accumulation gate V_g and oscillation frequency f at $T = 1.7 \text{ K}$. Amplitude color scale: 0.3 to 1. To obtain the FFT we use the raw $\Delta\rho_{xx}$ data with no background subtraction. Smoothing and interpolation are performed by using a Savitzky-Golay Matlab smoothing routine to obtain a $1/B$ equally spaced signal to feed into the FFT. (d) Comparison of densities from Hall effect and FFT analysis of the SdH oscillations as a function of accumulation gate V_g . n_1 (green) and n_2 (blue) are the single valley densities from FFT and $n_1 + n_2$ (black) is the resultant total density. n_H is the Hall density (red circles).

To quantify the population of the two valleys, we show in Fig. 2(c) the normalized fast Fourier transform (FFT) spectra amplitude of the oscillations as a function of V_g and oscillations frequency f . For $V_g \leq 4.6 \text{ V}$ we observe a single peak in the FFT spectra, pointing to a similar

population of the two valleys ($n_1 \sim n_2$) within the experimental resolution of the FFT. Because valley splitting grows with the valley population difference $\Delta n = n_1 - n_2$ [16,28,30,31],

$$\Delta E_{VS} = 2\epsilon_F \Delta n / n \quad (1)$$

where n is the total density, $\epsilon_F = \pi \hbar^2 n / m^*$ is the Fermi energy for spin-degenerate states and m^* is the effective mass in silicon, this is the regime characterized by a valley splitting smaller than the disorder-induced Landau level broadening $\Delta E_{VS} \leq \Gamma$ implying that beatings are not resolved in the SdH oscillations. Effectively, we measure transport through a single channel whose total density, and hence peak frequency, increases linearly with V_g . For $V_g \geq 4.6 \text{ V}$ we start to observe two distinct peaks at frequencies f_1 and f_2 because the increasing valley splitting overcomes the Landau level broadening. Correspondingly, two high mobility channels emerge in transport and beatings appear in the SdH oscillations [Fig. 2(b)]. We exclude intersubband resonant scattering [32,33] and treat these two channels independently since $f_1 \sim f_2$ in our measurements and we do not observe features associated to periodicity $f_1 - f_2$. The frequency separation between peaks $|(f_1 - f_2)|$, and hence $|(\Delta n)|$, grows with V_g , signaling an increasing valley splitting with electric field, in agreement with theoretical expectations [28,29,34]. Figure 2(d) shows the V_g -dependent carrier density in the two valleys n_1 and n_2 determined by the quantum Hall density vs peak frequency relationship $n_{1,2} = g_z g_v f_{1,2} (e/h)$, where e and h are the electron charge and the Planck's constant, $g_z = 2$ and $g_v = 1$ are Zeeman and valley degeneracy [35]. The total density determined by the FFT analysis of the SdH oscillations $n_1 + n_2$ (black) matches the Hall density n_H (red) obtained at low fields, confirming the validity of the two-band model for transport.

To extract valley splitting we use the following procedure. We identify the SdH oscillations showing clear beatings and fit the curves building upon the models reported in Refs. [28,30] that describe the quantum oscillations at low or intermediate magnetic fields with Lifshitz-Kosevich formulas [36]. The normalized oscillatory part of the magnetoresistance $\Delta\rho_{xx}/\rho_0$ is modeled as

$$\frac{\Delta\rho_{xx}}{\rho_0} = AC(\tau_q) \left[\cos\left(\frac{\beta}{B} n_1 - \pi\right) + \cos\left(\frac{\beta}{B} n_2 - \pi\right) \right], \quad (2)$$

where A is an amplitude prefactor that includes the spin degeneracy, $C(\tau_q)$ a term depending on the single particle relaxation time τ_q , as detailed below, and $\beta = \pi h/e$ a constant term. We use three fitting parameters. The first two fitting parameters are A and τ_q , that enter Eq. (2) via the temperature dependent term

$$C(\tau_q) = e^{-\frac{\pi}{\omega_c \tau_q}} \cdot \frac{2\pi^2 k_B T / \hbar \omega_c}{\sinh(2\pi^2 k_B T / \hbar \omega_c)} \cos\left(\frac{\pi g^* m^*}{2m_0}\right), \quad (3)$$

where we assume a spin susceptibility $g^* m^* / m_0 = 0.38$ in silicon and τ_q equal for the two valleys to minimize the number of fitting parameters, ω_c is the cyclotron frequency, k_B and \hbar are the Boltzmann and Planck constants. The third fitting parameter is the valley population difference Δn that enters Eq. (2) via the two valleys population $n_1 = (n + \Delta n)/2$ and $n_2 = (n - \Delta n)/2$, where n is the total density of the two valleys from Fig. 2(d). While A and C in Eq. (2) capture the overall shape of the curve, Δn influences the periodicity of the SdH oscillations and the interference patterns and is the key parameter to determine valley splitting via Eq. (1) [37].

Figure 3(a) shows, as an example of the fitting procedure, the experimental data $\Delta\rho_{xx}/\rho_0$ (black) from device B as a function of $1/B$, measured at high density ($n = 6.75 \times 10^{12} \text{ cm}^{-2}$) and at 1.7 K. Beating nodes are observed at $\sim 0.23 \text{ T}^{-1}$ ($\sim 4.45 \text{ T}$) and at $\sim 0.38 \text{ T}^{-1}$ ($\sim 2.63 \text{ T}$) and the fitted curve (red) matches well the

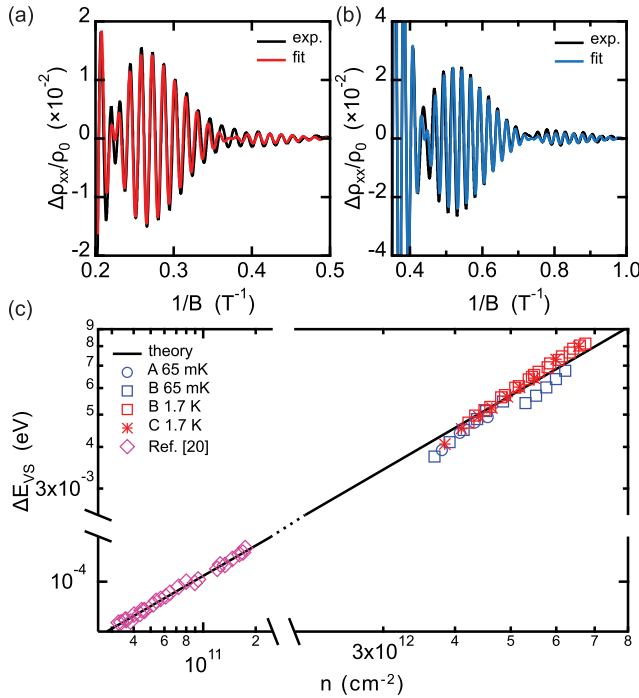


FIG. 3. Device B oscillations amplitude normalized to the low-field magnetoresistance $\Delta\rho_{xx}/\rho_{xx,0}$ as a function of inverse perpendicular field $1/B$ after smoothing and polynomial background subtraction (black) and their fittings (red and blue) at a temperature of (a) $T = 1.7 \text{ K}$ and (b) 65 mK . (c) Valley splitting ΔE_{VS} as a function of density n at a temperature of $T = 1.7 \text{ K}$ (red) and 65 mK (blue) from devices A (circles), B (squares) and C (asterisks). The black line is the theoretical density dependence of valley splitting $\Delta E_{VS} \sim 1.14 \times n$ where ΔE_{VS} and n are in meV and 10^{12} cm^{-2} units calculated in Ref. [34]. Magenta diamonds are experimental valley splitting values from Si/SiGe heterostructure-FET from Ref. [20].

experimental data. The fitted valley population difference $\Delta n = 3.2 \times 10^{11} \text{ cm}^{-2}$ corresponds to a valley splitting energy $\Delta E_{VS} = 8.2 \text{ meV}$. To improve on the temperature broadening of the oscillations, and better resolve the beatings, the sample is also cooled down to 65 mK . Figure 3(b) shows the experimental data (black) and the corresponding fitting (blue) at a lower density ($n = 3.93 \times 10^{12} \text{ cm}^{-2}$). The beatings nodes are better resolved and from the fitting parameter $\Delta n = 1.64 \times 10^{11} \text{ cm}^{-2}$ we obtain $\Delta E_{VS} = 4.1 \text{ meV}$, respectively [38]. Figure 3(c) summarizes the results of our fitting procedure and shows the valley splitting for Si-MOS devices A (circles), B (squares), and C (asterisks) estimated at $T = 1.7 \text{ K}$ (red) and 65 mK (blue) as a function of density in the range of 3.7 to $6.8 \times 10^{12} \text{ cm}^{-2}$. We compare our results with the experimental results (magenta diamonds, from Ref. [20]) and effective mass calculations (black line, from Ref. [34]) for valleys splitting in 2DEGs obtained in Si/SiGe heterostructures. Note that in the Si/SiGe heterostructures in Ref. [20] valley splitting was estimated by activation measurements in the quantum Hall regime. In Si-MOS, we observe large valley splitting energies that increase in the range of 3.7 to 8.2 meV near linearly with density, regardless of the device location on the wafer and temperature. This is in agreement with the observation of a uniform mobility at high density across devices pointing to a uniform semiconductor-dielectric interface across the wafer.

Crucially, we see that the valley splitting density dependence in Si-MOS extends to the high density regime the same trend that was observed in Si/SiGe at low density [20]. This trend is compatible [39] with the predicted density-dependent valley splitting calculated for a disorder-free Si/SiGe quantum well top interface [34]. From this observation we arrive at the following learning: The electron density, and hence the vertical electric field is the key parameter determining the measured valley splitting of 2DEGs in silicon in these wafers, regardless of the interface providing quantum confinement (Si/oxide in Si-MOS or Si/SiGe). We speculate that this apparent universal dependence of valley splitting upon density, and hence electric field, emerges in Hall bar measurements for the following two reasons. First, in a 2DEG the electric field is accurately determined as it connects directly to the measured density. Second, macroscopic Hall bar measurements average out the locally varying atomic-scale features at the confining interface that influence valley splitting variations in quantum dots.

In conclusion, we measured the density-dependent valley splitting in Si-MOS Hall-bar transistors made by advanced semiconductor manufacturing. Low disorder in these Hall bars allow to estimate valley splitting by analyzing the beating patterns arising from the two energy split valleys in magnetotransport. Comparing the data with previous theory and experimental work for 2DEGs in Si, we highlight the critical role of vertical electric field in determining valley splitting.

Data sets supporting the findings of this study are available [40].

- *g.scappucci@tudelft.nl
- [1] F. A. Zwanenburg, A. S. Dzurak, A. Morello, M. Y. Simmons, L. C. L. Hollenberg, G. Klimeck, S. Rogge, S. N. Coppersmith, and M. A. Eriksson, *Rev. Mod. Phys.* **85**, 961 (2013).
- [2] M. Veldhorst, J. C. C. Hwang, C. H. Yang, A. W. Leenstra, B. de Ronde, J. P. Dehollain, J. T. Muhonen, F. E. Hudson, K. M. Itoh, A. Morello, and A. S. Dzurak, *Nat. Nanotechnol.* **9**, 981 (2014).
- [3] M. Veldhorst, C. H. Yang, J. C. C. Hwang, W. Huang, J. P. Dehollain, J. T. Muhonen, S. Simmons, A. Laucht, F. E. Hudson, K. M. Itoh, A. Morello, and A. S. Dzurak, *Nature (London)* **526**, 410 (2015).
- [4] L. M. K. Vandersypen and M. A. Eriksson, *Phys. Today* **72**, 38 (2019).
- [5] C. H. Yang, K. W. Chan, R. Harper, W. Huang, T. Evans, J. C. C. Hwang, B. Hensen, A. Laucht, T. Tantt, F. E. Hudson, S. T. Flammia, K. M. Itoh, A. Morello, S. D. Bartlett, and A. S. Dzurak, *Nat. Electron.* **2**, 151 (2019).
- [6] W. Huang, C. H. Yang, K. W. Chan, T. Tantt, B. Hensen, R. C. C. Leon, M. A. Fogarty, J. C. C. Hwang, F. E. Hudson, K. M. Itoh, A. Morello, A. Laucht, and A. S. Dzurak, *Nature (London)* **569**, 532 (2019).
- [7] C. H. Yang, R. C. C. Leon, J. C. C. Hwang, A. Saraiva, T. Tantt, W. Huang, J. Camirand Lemyre, K. W. Chan, K. Y. Tan, F. E. Hudson, K. M. Itoh, A. Morello, M. Pioro-Ladrière, A. Laucht, and A. S. Dzurak, *Nature (London)* **580**, 350 (2020).
- [8] L. Petit, H. G. J. Eenink, M. Russ, W. I. L. Lawrie, N. W. Hendrickx, S. G. J. Philips, J. S. Clarke, L. M. K. Vandersypen, and M. Veldhorst, *Nature (London)* **580**, 355 (2020).
- [9] X. Xue *et al.*, *Nature (London)* **593**, 205 (2021).
- [10] A. M. J. Zwerver *et al.*, *Nat. Electron.* **5**, 184 (2022).
- [11] D. Sabbagh *et al.*, *Phys. Rev. Applied* **12**, 014013 (2019).
- [12] B. Paquelet Wuetz, P. L. Bavdaz, L. A. Yeoh, R. Schouten, H. van der Does, M. Tiggelman, D. Sabbagh, A. Sammak, C. G. Almudever, F. Sebastiano, J. S. Clarke, M. Veldhorst, and G. Scappucci, *npj Quantum Inf.* **6**, 43 (2020).
- [13] F. F. Fang and W. E. Howard, *Phys. Rev. Lett.* **16**, 797 (1966).
- [14] F. Stern and W. E. Howard, *Phys. Rev.* **163**, 816 (1967).
- [15] L. J. Sham and M. Nakayama, *Phys. Rev. B* **20**, 734 (1979).
- [16] T. Ando, A. B. Fowler, and F. Stern, *Rev. Mod. Phys.* **54**, 437 (1982).
- [17] C. H. Yang, A. Rossi, R. Ruskov, N. S. Lai, F. A. Mohiyaddin, S. Lee, C. Tahan, G. Klimeck, A. Morello, and A. S. Dzurak, *Nat. Commun.* **4**, 2069 (2013).
- [18] L. Petit, J. M. Boter, H. G. J. Eenink, G. Droulers, M. L. V. Tagliaferri, R. Li, D. P. Franke, K. J. Singh, J. S. Clarke, R. N. Schouten, V. V. Dobrovitski, L. M. K. Vandersypen, and M. Veldhorst, *Phys. Rev. Lett.* **121**, 076801 (2018).
- [19] L. A. Tracy, K. Eng, K. Childs, M. S. Carroll, and M. P. Lilly, *Solid State Commun.* **150**, 231 (2010).
- [20] B. Paquelet Wuetz, M. P. Losert, A. Tosato, M. Lodari, P. L. Bavdaz, L. Stehouwer, P. Amin, J. S. Clarke, S. N. Coppersmith, A. Sammak, M. Veldhorst, M. Friesen, and G. Scappucci, *Phys. Rev. Lett.* **125**, 186801 (2020).
- [21] R. Pillarisetty *et al.*, in *2021 IEEE International Electron Devices Meeting (IEDM)*, (IEEE, San Francisco, CA, USA 2021), pp. 14.1.1–14.1.4.
- [22] M. Lodari, N. W. Hendrickx, W. I. L. Lawrie, T.-K. Hsiao, L. M. K. Vandersypen, A. Sammak, M. Veldhorst, and G. Scappucci, *Mater. Quantum Technol.* **1**, 011002 (2021).
- [23] L. A. Tracy, E. H. Hwang, K. Eng, G. A. Ten Eyck, E. P. Nordberg, K. Childs, M. S. Carroll, M. P. Lilly, and S. Das Sarma, *Phys. Rev. B* **79**, 235307 (2009).
- [24] Since the percolation theory is only valid close to the turn-on threshold, a fitting density range as small as $1.3 \times 10^{11} \text{ cm}^{-2}$ is used.
- [25] T. N. Camenzind, A. Elsayed, F. A. Mohiyaddin, R. Li, S. Kubicek, J. Jussot, P. V. Dorpe, B. Govoreanu, I. Radu, and D. M. Zumbühl, *Mater. Quantum Technol.* **1**, 041001 (2021).
- [26] J.-S. Kim, A. M. Tyryshkin, and S. A. Lyon, *Appl. Phys. Lett.* **110**, 123505 (2017).
- [27] A single particle relaxation time $\tau_q = (0.65 \pm 0.02) \text{ ps}$ is extracted from the SdH oscillations envelope, corresponding to a Landau levels broadening of $\Gamma = 508 \mu\text{eV}$, that is, qualitatively, a lower boundary to the VS that can be resolved in magnetotransport.
- [28] V. M. Pudalov, A. Punnoose, G. Brunthaler, A. Prinz, and G. Bauer, <https://arxiv.org/abs/cond-mat/0104347> (2001).
- [29] M. V. Chermisin, *Int. J. Mod. Phys. B* **18**, 3609 (2004).
- [30] A. Isihara and L. Smrcka, *J. Phys. C* **19**, 6777 (1986).
- [31] K. Takashina, Y. Ono, A. Fujiwara, Y. Takahashi, and Y. Hirayama, *Phys. Rev. Lett.* **96**, 236801 (2006).
- [32] D. R. Leadley, R. Fletcher, R. J. Nicholas, F. Tao, C. T. Foxon, and J. J. Harris, *Phys. Rev. B* **46**, 12439 (1992).
- [33] P. T. Coleridge, *Semicond. Sci. Technol.* **5**, 961 (1990).
- [34] M. Friesen, S. Chutia, C. Tahan, and S. N. Coppersmith, *Phys. Rev. B* **75**, 115318 (2007).
- [35] When the valley splitting is not resolved ($V_g < 4.6 \text{ V}$) we assume equal population of the two valleys.
- [36] I. M. Lifshits and A. M. Kosevich, *Zh. Eksp. Teor. Fiz.* **29**, 730 (1955) [*Sov. Phys. JETP* **2**, 636 (1956)].
- [37] As an initial guess of the fitting procedure we use the density difference $\Delta n = |n_1 - n_2|$ values obtained via FFT, $A = 1$, and $\tau_q = 0.5 \text{ ps}$ for the valley population difference, the amplitude, and the single particle relaxation time, respectively. Since A and τ_q are not relevant for the valley splitting determination, they are not further discussed in the rest of this work. Nonetheless, values of τ_q compatible with those extracted from the Dingle plot close to peak mobility are found in the range 0.42–0.16 ps for increasing densities.
- [38] We do not see an increase of the amplitude modulation of beatings in the Shubnikov–de Haas oscillations with increasing temperature, confirming the absence of intersubband resonant scattering.
- [39] A linear fit of all the ΔE_{VS} data for Si-MOS results in a slope for the valley splitting density dependence of $(1.15 \pm 0.02) \text{ meV} \times 10^{-12} \text{ cm}^2$. The linear fitting intercept has been fixed to 0.
- [40] [10.4121/17136608.v1](https://doi.org/10.4121/17136608.v1).